Beta bursts in SMA mediate anticipatory muscle inhibition in a bimanual postural task

Abbreviated title: SMA beta bursts mediate anticipatory inhibition

V. Manyukhina[1], O. Abdoun[1], F. Di Rienzo[1,2], F. Barlaam[1], S. Daligault[3], C. Delpuech[1,3], Maciej Szul[4,5,6], James Bonaiuto[4,5], M. Bonnefond[1]**, C. Schmitz[1]**

**both authors equally contributed to the work

[1]Université Claude Bernard Lyon 1, CNRS, INSERM, Centre de Recherche en Neurosciences de Lyon CRNL U1028 UMR5292, COPHY, F-69500, Bron, France

[2]Université de Lyon, Université Claude Bernard Lyon 1, Laboratoire Interuniversitaire de Biologie de la Motricité-UR 7424, F-69100, Villeurbanne, France

[3]CERMEP-Imagerie du Vivant, MEG Departement, F-69500, Bron, France

[4]Université de Lyon, Université Claude Bernard Lyon 1, F-69100, Villeurbanne, France

[5]Institut des Sciences Cognitives Marc Jeannerod, CNRS, UMR5229, F-69500, Bron, France

[6]Department of Psychiatry and Psychotherapy, Faculty of Medicine, University of Tübingen, 72076 Tübingen, Germany

Corresponding authors: vimanyukhina@gmail.com, mathilde.bonnefond@inserm.fr

Number of pages: 61

Number of figures: 4

Number of tables: 3

Number of words: Abstract (250/250), Introduction (650/650), Discussion (1500/1500)

Conflict of interest: The authors declare no conflict of interest.

Acknowledgments: The authors would like to thank Jérôme Prado, Franck Lamberton, and Sarah Le Diagon for their valuable contributions to this study, as well as the staff of CERMEP–Imagerie du Vivant for their helpful assistance with data collection. This study was supported by funding from the French National Research Agency: ANR SaMenta ASD-BARN (ANR-12-SAMA-015-01), LABEX CORTEX (ANR-11-LABX-0042) of Université de Lyon, within the program "Investissements d'Avenir" (ANR-11-IDEX-0007). Viktoriya Manyukhina was funded by a scholarship from the French Ministry of Research.

Abstract

Motor anticipation is essential for accurate and coordinated hand movements in humans. A valuable framework to study it is provided by the Bimanual Load-Lifting Task (BLLT), in which voluntarily lifting a load supported by the opposite forearm is preceded by anticipatory inhibition of the elbow flexors in the supporting arm, preventing forearm instability. In sixteen adult participants performing the BLLT, we recorded magnetoencephalography (MEG) to investigate the neural mechanisms underlying anticipatory inhibition. Optimal postural stabilization was observed when the elbow flexor was inhibited around 30 ms before unloading. Stronger muscle inhibition in this optimal time interval was associated with reduced excitability – indexed by high-gamma (90-130 Hz) power – and increased high-beta (18-25 Hz) power in the contralateral Supplementary Motor Area (SMA). Mediation analysis revealed that high-gamma power reduction significantly mediates the relationship between high-beta power and anticipatory inhibition. We further showed that trials containing beta

bursts (22-28 Hz) exhibit optimally timed anticipatory inhibition and a concurrent decrease in high-gamma power. Directed connectivity analysis using the Phase Slope Index demonstrated that these beta bursts propagate to the SMA from the lateral prefrontal cortex (lPFC) and the elbow-related primary motor cortex (M1), both of which increase their burst probability during SMA bursts. Together, our findings suggest that, during voluntary load-lifting, optimal anticipatory muscle inhibition in the load-supporting forearm is achieved through reduced SMA excitability, mediated by beta bursts originating from an lPFC-M1-SMA network. To our knowledge, this also provides the first direct evidence that beta-band activity can exert inhibitory control over muscle function.

Significance statement

Anticipatory motor control evolved in humans to perform precise, coordinated voluntary movements by compensating for the postural perturbations they generate. We investigated this behaviour using a bimanual postural task, in which accurate lifting of a load supported by the forearm relies on the anticipatory inhibition of ongoing postural command in the elbow flexors of the supporting arm. Our results suggest that beta bursts (22-28 Hz) mediate optimal anticipatory inhibition by suppressing activity in the Supplementary Motor Area associated with the initial control of the forearm, i.e., prior to load-lifting. These findings shed light on the neural mechanisms of motor anticipation and, to our knowledge, provide the first direct evidence that beta-band activity can exert inhibitory control over muscle function.

Introduction

Many voluntary movements cause postural perturbations that can be compensated by adjusting postural muscles before movement. A common example is the “waiter task”: when a waiter holds a tray of glasses and is about to take one with his other hand, the brain must adapt to the upcoming force changes on the tray-bearing arm to avoid spillage. This behaviour is achieved through anticipatory postural adjustments (APA), which are integral to our daily lives and are characterized by being initiated before the onset of movement, minimizing its destabilizing effects on posture (Massion, 1992). A commonly used naturalistic paradigm for studying APA in humans is the bimanual load-lifting task (BLLT), which mimics the waiter task (Hugon et al., 1982). In the BLLT, a load is placed on the wrist of the supporting arm, whose elbow is fixed to allow only up-and-down movement, while the participant lifts the load using the other hand. The unloading induces a change in force, leading to destabilization of the postural arm, observed as an upward forearm movement. APA, which are generated before the object is lifted, stabilize the forearm thereby minimizing perturbation. In contrast, unexpected unloading causes a pronounced upward elbow rotation, followed by reflexive inhibition that stabilizes posture (Hugon et al., 1982).

APA result from precise brain-level coordination between postural and motor commands, requiring the engagement of the same muscles on both the postural and lifting sides (Paulignan et al., 1989; Kaluzny and Wiesendanger, 1992). Another key feature of APA is the inhibition of elbow flexor activity, reflected as a decrease in electromyography (EMG) signal. This muscle inhibition precedes unloading and

contributes to the horizontal stabilization of the forearm during load-lifting, ensuring a smooth transition to a new equilibrium. The precise timing of this muscle inhibition is crucial for effective bimanual coordination (Hugon et al., 1982; Viallet et al., 1987). Impaired APA, measured using the BLLT, have been observed in Parkinson's disease (Viallet et al., 1987), Autism Spectrum Disorders (Schmitz et al., 2003), and other developmental motor-related conditions (Jover et al., 2006, 2010).

The network and oscillatory mechanisms underlying APA, specifically anticipatory muscle inhibition, remain poorly understood. The BLLT, which allows spatial separation of motor and postural commands across hemispheres, offers a valuable framework for investigating APA generation, which can provide a basis for examining its alterations in motor disorders. Given the explicit muscle inhibition observed in BLLT, it may also advance our understanding of how inhibitory control is implemented in the brain. In this study, we therefore aimed to examine the mechanisms underlying anticipatory muscle inhibition and to characterize the neural network supporting it.

In motor networks, inhibition is hypothesized to be mediated by oscillatory activity in the mu (8-12 Hz) and beta (13-30 Hz) frequency bands. Elevated mu power has been associated with the inhibition of motor actions, preventing their execution (Bönstrup et al., 2015; Köster and Meyer, 2023). Beta-band activity, predominantly observed in bursts (Lundqvist et al., 2024), has been implicated in the inhibition (Picazio et al., 2014; Schaum et al., 2020; Enz et al., 2021) or slowing (Khanna and Carmena, 2017; Little et al., 2019) of motor actions. Here, we investigated whether anticipatory muscle inhibition in a bimanual postural task is mediated by alpha- or beta-band activity.

Motor inhibition has been linked to reduced activity in the primary motor cortex (M1) in previous studies (Kazennikov et al., 2005, 2006; Borgomaneri et al., 2020). However, in the BLLT, Ng et al., (2013a) observed more pronounced beta desynchronization in the supplementary motor area (SMA) contralateral to the load-supporting arm than in M1 before unloading, and speculated that corticospinal projections from the SMA may play a central role in APA regulation. We therefore aimed to investigate whether anticipatory elbow flexor inhibition during BLLT is accompanied by decreased M1 or SMA activity, and to identify the network conveying this inhibitory signal, potentially involving the prefrontal cortex or subcortical structures such as the basal ganglia or cerebellum.

Methods

Participants

Sixteen right-handed adults without neurological or psychiatric conditions (11 males, mean age 27 ± standard deviation (SD) 3.8 years) participated in this study. Handedness was determined using the Edinburgh Handedness Inventory (Oldfield, 1971). All participants gave written informed consent in accordance with the Declaration of Helsinki. The study was approved by the local ethics committee (South East IV Committee for the Protection of Persons). A study involving the same participants, but examining learning mechanisms in a different task during the same experimental session, has previously been published (Di Rienzo et al., 2019).

Experimental setting and task

The experimental setup of the BLLT, while recording brain activity using EEG (Barlaam et al., 2011) or MEG (Di Rienzo et al., 2019), has been described in more detail elsewhere. In short, while participants were seated under the MEG helmet, their left arm was positioned adjacent to the trunk, with the elbow resting on a support and fixed to allow only upward and downward rotations. They were instructed to maintain the left forearm in a horizontal semi-prone position, as if supporting a tray. This instruction implicitly defined the reference frame to be preserved during lifting. A non-magnetic wristband fitted with a vacuum switch system (30 kN/m^2) strain gauge was

worn on the wrist, allowing an 850g load to be placed on top of it (in the voluntary unloading condition), or suspended, with the possibility of being released by 3.5 kN/m^2 air pulses (in the imposed unloading condition).

In the voluntary unloading condition, the participants positioned their right hand above the object to be lifted. Each trial started with a two-second fixation on a light spot projected onto the wrist to limit eye movements during lifting. Upon light extinction (fade-out), participants were instructed to lift the load placed on top of the wristband at any time, raising it up to approximately ten centimeters above the device. After a few seconds of holding the load, participants had to return it to its initial position, completing the trial. Since participants performed the unloading themselves, the use of APA resulted in minimal forearm destabilization, reflected in low elbow rotation, following unloading. In this condition, APA are characterized by anticipatory EMG inhibition in the forearm flexor muscles (*Biceps brachii* and *Brachioradialis*), which typically occurs just before the onset of unloading (Hugon et al., 1982; Barlaam et al., 2011).

In the imposed (control) unloading condition, the experimenter released the load at a random time after light extinction, making the use of APA impossible. In contrast to voluntary unloading, imposed unloading results in a significant passive upward rotation of the elbow, and inhibition of the forearm flexor muscles after unloading onset, known as the unloading reflex (Hugon et al., 1982; Schmitz et al., 2002).

In total, there were 90 trials in both the imposed and voluntary unloading conditions. To reduce fatigue, they were organized into sessions of 10 trials each, with intervals of around 1 minute between the sessions.

Behavioural data acquisition

Detection of load-lifting timing

The onset of load-lifting (unloading, zero reference time point) was automatically identified as the initial deflection in the force signal recorded by the force plate sensor attached to the non-magnetic wristband, using a threshold function in CTF® DataEditor software. The automatically assigned label was then visually inspected and manually corrected if needed.

Elbow-joint rotation

Upward rotation of the elbow joint following load release or lifting was measured across all trials and conditions using a copper potentiometer aligned with the elbow joint axis and sampled at 20 kHz. The signal was resampled at 600 Hz for analysis. The deflection amplitude was recorded in arbitrary units provided by the equipment.

Electromyography

Electromyography (EMG) data were collected at a sampling frequency of 600 Hz using bipolar surface electrodes (2.5 mm^2 surface area) positioned over the left

Brachioradialis, *Biceps brachii*, and *Triceps brachii* on the postural side, as well as the right arm *Biceps brachii*. For the purposes of this study, only EMG data from the left *Biceps brachii* were analyzed.

Behavioural data preprocessing

Elbow rotation

To evaluate postural stabilization as an indicator of APA efficacy in the voluntary unloading condition, we introduced two metrics: Peak Elbow Rotation and Elbow Rotation Decline, representing the two principal directions of forearm destabilization (see Figure 2A, left panel). We assumed that in trials when APA are effective, both Peak Elbow Rotation and Elbow Rotation Decline would exhibit values close to zero, indicating optimal postural stabilization.

To estimate Peak Elbow Rotation and Elbow Rotation Decline in the voluntary unloading condition, the elbow rotation time series were first smoothed using a moving average filter with a window of 5 time points (8.3 ms) and a step size of 1 time point (1.7 ms) to reduce noise. The time point of maximal elbow deflection was visually identified in the time series using the ‘annotations’ tool in MNE-Python and was subsequently used to estimate Peak Elbow Rotation (see below). This step was performed manually because, in most trials, the peak elbow rotation was very small and difficult to reliably detect using automatic algorithms. The time series were then epoched from -

1.7 to 1.2 s relative to the annotated time point of maximum elbow rotation.

The amplitude of Elbow Rotation Decline was defined as the difference between the average of the minimum values corresponding to 33 ms (excluding outliers) in the time interval from -0.165 to 0 s relative to the start of unloading, and the average of the same number of maximal values (baseline interval) in the time interval from -0.165 s to the first time point selected for averaging the minimum values. This ensured exclusion of the subsequent positive elbow deflection. Therefore, in case of negligible elbow decline, time intervals for Elbow Rotation Decline and its baseline could overlap.

The amplitude of Peak Elbow Rotation was calculated as the average of baseline-corrected values within a 33 ms window surrounding the maximal elbow deflection, excluding outliers. The baseline for each trial was defined as the average of the minimum values corresponding to 33 ms (excluding outliers) in the time interval from -0.35 to -0.05 s relative to the onset of unloading.

Overall, Elbow Rotation Decline and Peak Elbow Rotation values were calculated individually for each trial. The resulting plots for each trial, including the time points used to estimate peak elbow rotation, elbow rotation decline, and their respective baselines, were visually inspected. Figure 1B illustrates three example trials with their corresponding analysis windows. Trials containing severe artifacts that precluded reliable estimation of elbow rotation measures were identified and excluded. The number of such trials per participant ranged from 0 to 5 (mean = 1.25, SD = 1.39). All analyses involving elbow rotation data were conducted on the remaining artifact-free trials.

In the imposed condition, to assess the postural destabilization triggered by the experimenter's unexpected release of the load, upward elbow rotation was measured using Peak Elbow Rotation only, as Elbow Rotation Decline was not observed in this condition. Peak Elbow Rotation was defined as in the voluntary condition (see above), except that the prominent peak in elbow rotation allowed for automatic detection as a maximum within the trial window.

Electromyography (EMG)

For this study, EMG recordings from the left *Biceps brachii* were analyzed. Preprocessing followed established protocols (Schmitz et al., 2002; Barlaam et al., 2011, 2018) and included epoching from -1 to 0.5 s relative to the onset of unloading, mean subtraction, and band-pass filtering using a finite impulse response (FIR) filter with a Hamming window in the 25-150 Hz range. This frequency range was selected based on inspection of group-averaged muscle power spectral density. The filtered signals were then rectified to enable visualization of EMG inhibition as a reduction in EMG power (see Figure 2A, right panel). After log10-transformation and baseline correction (-1 to -0.5 s), the EMG signal was smoothed using a 30 ms moving average with 33% overlap to improve the reliability of inhibition estimates.

Estimation of the EMG inhibition

Since high noise levels in the EMG signal prevented accurate trial-by-trial assessment of muscle inhibition, we instead aimed to quantify inhibition strength during the period

in which it most effectively contributed to subsequent postural stabilization – specifically, when inhibition was followed by the maintenance of a stable horizontal forearm position. This involved identifying the time interval in which EMG inhibition had the strongest effect on both Elbow Rotation Decline and Peak Elbow Rotation, bringing both values close to zero.

The anticipatory muscle inhibition observed in this paradigm likely reflects the suppression, or adjustment, of the central motor command responsible for flexor muscle contraction, finely tuned to maintain the forearm in a horizontal position despite the opposing force exerted by the load. Its effectiveness depends critically on timing, which must be optimal: not too early, to ensure forearm stability until the load is released, and not too late, to prevent destabilization caused by the sudden change in force. Figure 1A provides a schematic overview of these timing scenarios – early, on-time, and late – and their expected behavioral effects.

To investigate the mechanisms underlying the most efficient strategy, i.e. on-time inhibition, which is predominant in adult participants (Schmitz et al., 2002), we aimed to determine the time at which EMG inhibition results in the smallest negative deflection (Elbow Rotation Decline) before unloading and lowest Peak Elbow Rotation after unloading (option 1, Figure 1A).

To this end, we fitted a linear regression model for each participant across trials, using Elbow Rotation Decline and Peak Elbow Rotation as predictors of EMG inhibition. The OLS() function from statsmodels.regression.linear_model module (statsmodels library, v. 0.14.1) was used to fit a separate linear regression model at each time point of the smoothed EMG signal (see above). The F-value was used as the evaluation metric for each regression model, and the coefficient of determination (R^2) was used to assess

the quality of the prediction. F-values were log10-transformed to normalize their distribution and baseline-corrected (-1 to -0.5 s). Therefore, positive baseline-corrected F-values indicated time intervals where Elbow Rotation Decline and Peak Elbow Rotation most strongly predicted *Biceps brachii* inhibition, relative to baseline activity. A one-sample permutation cluster test was used to assess whether the positive, baseline-corrected F-values significantly differed from zero across subjects, within the time interval of -0.25 to 0.1 s relative to unloading, with clustering based on temporal adjacency.

In the imposed condition, where anticipating load release was impossible, the unloading reflex – characterized by *Biceps brachii* inhibition – occurred approximately 100 ms after unloading. To detect muscle activity decrease in each participant, EMG data were preprocessed following the same steps as in the voluntary condition and baseline-corrected (-1 to -0.5 s). For each participant, EMG inhibition strength was derived by averaging the signal within a 30 ms window around the latency at which the greatest inhibition occurred in the trial-averaged data.

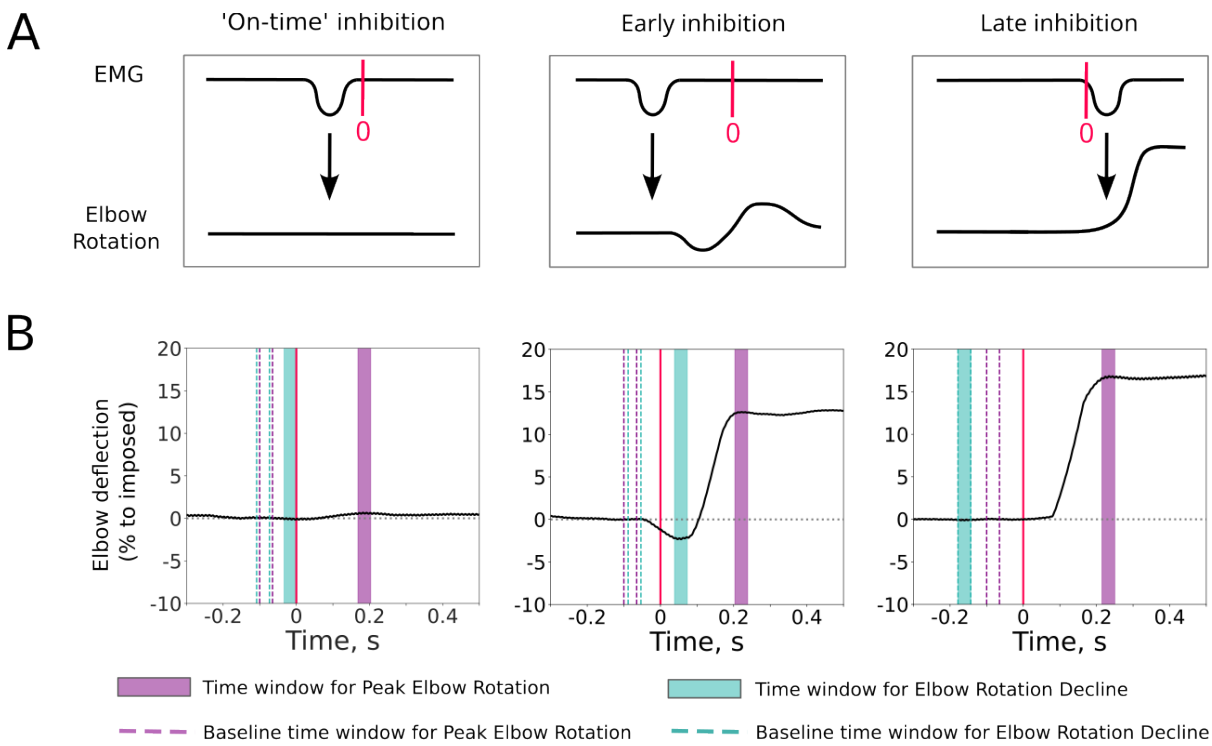

Figure 1. Estimating elbow deflection and its expected relationship to the timing of *Biceps brachii* inhibition. **A:** Schematic illustration of three primary possible scenarios for *Biceps brachii* inhibition timing and its impact on elbow rotation. See Methods (section *Estimation of the EMG inhibition*) for a detailed explanation. **B:** Single-trial examples showing the time intervals used to estimate Peak Elbow Rotation and Elbow Rotation Decline. Values are presented as percentages of elbow rotation during voluntary unloading relative to the individual maximum, estimated as the median peak elbow rotation in the imposed condition.

MRI data acquisition and preprocessing

Structural magnetic resonance imaging (MRI; voxel size 0.9 mm x 0.9 mm x 0.9 mm; TR=3500 ms, TE=2.24 ms) data were obtained from all participants using a 3T Siemens

Magnetom scanner (CERMEP, France - MAGNETOM Prisma, Siemens HealthCare). T1-weighted images were preprocessed with the ‘recon-all’ procedure from FreeSurfer software (version 6.0.0; Fischl et al., 2002), which includes motion correction, intensity normalization, removal of non-brain tissue, cortical surface reconstruction, and subcortical segmentation.

The cortical surface was parcellated into 450 regions using the "HCPMMP1" atlas (Glasser et al., 2016), as implemented in MNE-Python software (v. 1.7.0; Gramfort et al., 2013). Source-level MEG analysis was then restricted to right-hemisphere motor network areas involved in anticipatory motor control of the left forearm, particularly those previously associated with voluntary unloading in the BLLT task (Schmitz et al., 2005; Ng et al., 2011, 2013a, 2013b), see Table 1.

In addition to cortical regions, several subcortical structures in the right hemisphere implicated in the BLLT task were included in the MEG source-level analysis. These regions were automatically parcellated using the Aseg atlas in FreeSurfer and included the cerebellar cortex and basal ganglia (caudate nucleus, putamen, and globus pallidus).

	Cortical parcellation labels from Glasser et al. (2016)
M1	R_4_ROI
SMA	R_SCEF_ROI, R_6ma_ROI, R_6mp_ROI
PM	R_55b_ROI, R_6d_ROI, R_6a_ROI
CMA	R_24dd_ROI, R_24dv_ROI

PrCu	R_PCV_ROI, R_7Am_ROI, R_7Pm_ROI
SMar	R_PF_ROI, R_Pft_ROI, R_Pfop_ROI, R_Pfm_ROI, R_PFcm_ROI
dlPFC	R_8C_ROI, R_8Av_ROI, R_i6-8_ROI, R_s6-8_ROI, R_SFL_ROI, R_8BL_ROI, R_9p_ROI, R_9a_ROI, R_8Ad_ROI, R_p9-46v_ROI, R_a9-46v_ROI, R_46_ROI, R_9-46d_ROI
IFC*	R_44_ROI, R_45_ROI, R_IFJp_ROI, R_IFJa_ROI, R_IFSp_ROI, R_IFSa_ROI, R_47l_ROI, R_p47r_ROI

Table 1. Regions of interest (ROIs) selected for MEG source-level analysis, representing key nodes of the right anticipatory motor network.
Primary motor cortex, M1; supplementary motor area, SMA; premotor cortex, PM; cingulate motor area, CMA; precuneus, PrCu; supramarginal gyrus, SMar; dorsolateral prefrontal cortex, dlPFC; inferior frontal cortex, IFC.
* IFC involvement was not observed in the BLLT task, however it was included in the connectivity analysis due to its well-established role in inhibitory motor control (Swann et al., 2012; Xu et al., 2016).

MEG data acquisition

Magnetoencephalography (MEG) recordings were acquired using a CTF-MEG system (CERMEP, France - CTF MEG Neuro Innovations, Inc), equipped with 275 radial gradiometers positioned to cover the scalp, along with 29 reference channels for

correcting ambient noise. The MEG signals were digitized at a 600 Hz sampling rate and low-pass filtered between 0 and 150 Hz. Head position was tracked continuously using three coils placed on the nasion and preauricular points before recording.

MEG sensor-level data analysis

Preprocessing steps

MEG data preprocessing and analysis were performed using MNE-python software (v. 1.7.0; Gramfort et al., 2013). Raw MEG data from the voluntary unloading condition (three sessions per participant), aligned to the initial head position within each session, were concatenated. Visual inspection confirmed that head movements did not exceed 1 cm along the x, y, or z axes. A detailed analysis further showed that head position remained stable across all three coordinates during the anticipatory period (-0.5 to 0 s relative to unloading), which was used in subsequent analyses.

The data were high-pass filtered at 1 Hz before applying Independent Component Analysis (ICA) using the ICA() function (number of components: 70, method: 'picard', maximum number of iterations: 1000, reference channels were included in the IC estimation). Components reflecting biological artifacts (blinks, heartbeat, muscle activity) were identified and excluded based on visual inspection of their time courses and topographies. To detect components contaminated by intermittent environmental noise, MEG reference channels were used with the

find_bads_ref() function (threshold=1.5). Identified components were then removed from the unfiltered copy of the raw data. The average number of excluded components (mean ± SD) was as follows: EOG-related: 2.06 ± 0.24; ECG-related: 1.25 ± 0.56; EMG-related: 1.44 ± 1.54; artifact noise: 6.56 ± 3.46.

The raw data were epoched from -1.7 to 1.2 s relative to unloading onset. Only trials in which the unloading onset was detectable and the elbow rotation signal did not exhibit severe artifacts were included (number of dropped trials per subject, mean ± SD: 1.19 ± 1.18). Data of 275 axial gradiometers were selected for the analysis. Epochs were visually inspected and those contaminated by instrumental noise and myogenic artifacts were excluded (number of dropped trials per subject, mean ± SD: 2.00 ± 2.89). Several trials were additionally excluded from the elbow rotation analyses due to the presence of artifacts in time intervals critical for reliably estimating Peak Elbow Rotation and/or Elbow Rotation Decline (see above). The final average number of trials per participant was 86.94 ± 2.97 (mean ± SD).

For the imposed (control) condition, preprocessing included the same steps, with epoching performed in the time interval of -0.5 to 0.5 s relative to unloading onset, resulting in a total of 87.00 ± 5.55 (mean ± SD) trials per subject.

MEG source-level data analysis

Individual brain models and inverse solution

Three MRI-visible fiducial landmarks (nasion, left auricular, and right auricular) were manually positioned and used to define the head coordinate system. Individual structural MRI data were coregistered with the MEG raw data using the mne.gui.coregistration() tool. A single-layer boundary element model (BEM) was created with 20,484 vertices across both hemispheres. A mixed source space was defined, combining a surface-based source space with 'ico4' spacing yielding 5,124 cortical vertices in both hemispheres and a volume source space with 5 mm spacing, which included the cerebellum and basal ganglia comprising a total of 1,300 sources. The forward solution was computed for sources with a minimal distance of 5 mm from the inner skull surface.

Notch filters at 50 and 100 Hz were applied to the raw data after ICA to reduce powerline noise. The data were then band-pass filtered in the 25-150 Hz range for gamma activity analysis, and in the 1-90 Hz range for alpha-beta power analysis. Both filters used FIR filtering with a Hamming window and zero-phase configuration. The filter length was set to 'auto' using the 'firwin' design, with a 'reflect_limited' padding type. The resulting data were epoched as described in the preprocessing step, and bad trials were excluded based on prior annotations.

The data rank was computed from the epoched data, with the singular value tolerance for considering non-zero values set to 1e-6 and the tolerance kind set to ‘relative’. The data covariance matrix was then calculated for the time interval from -1 to 0.1 s relative to unloading onset, which was expected to capture the brain response associated with anticipatory motor control. This covariance matrix was computed using the estimated rank and the ‘empirical’ method. Since only gradiometer channels were used and the beamformer approach was adopted, noise covariance estimation for

source reconstruction was not necessary. A unit-gain Linearly Constrained Minimum Variance (LCMV) beamformer spatial filter was computed to optimize power orientation, with a regularization coefficient of 0.05 and enabling the rank reduction. The resulting filter was applied to each epoch individually.

Time-frequency analysis

Time-frequency analysis was performed over the full time window from -1.7 to 1.2 s, with symmetric padding of 0.5 s added on both sides of the time array. The resulting data were then cropped to the window of interest (-0.5 to 0.25 s) relative to unloading.

For gamma power estimation, the Multitaper method (using the tfr_array_multitaper() function) was applied to the time series of individual-trial source activity reconstructed with the LCMV beamformer. The analysis was conducted in the 90-130 Hz frequency range, using 7 cycles, a time_bandwidth parameter of 4, and a frequency resolution of 1 Hz. The resulting power estimates were log10-transformed and averaged across the frequency dimension to yield a mean high-gamma power estimate for the 90-130 Hz band.

For power estimation in the alpha-beta range, the Superlets algorithm was used (https://github.com/irhum/superlets; Moca et al., 2021). For each trial and brain source, the superlets() Python function was applied to the time series within the 1-80 Hz frequency range, with the base cycle set to 3. Adaptive superlet orders ranged from 1 to 20.

Periodic activity was separated from the total 1-80 Hz power using the Specparam tool (‘FOOOF’; Donoghue et al., 2020). The fitting range of 2-80 Hz was

determined through visual inspection of spectral densities from trial-averaged sources. Periodic power per trial and source was computed as the difference between the total power and the aperiodic fit estimated by the Specparam model, derived from trial-averaged spectra. For further analysis, the 8–30 Hz alpha-beta band was extracted.

Correlational analyses

Previous studies suggest that anticipatory flexor muscle inhibition during voluntary unloading may be attributed to reduced excitability, rather than enhanced inhibitory drive, in the brain regions governing muscle control (Kazennikov et al., 2005, 2006). To test this, we used Spearman's rank correlation to relate anticipatory inhibition estimate (EMG inhibition, see Results) to high-gamma power (90-130 Hz), used as a proxy for cortical excitability. High-gamma activity – typically defined as neural activity within a broad frequency range above 60 or 80 Hz – has been shown to correlate closely with neuronal spiking in both sensory (Ray et al., 2008; Ray and Maunsell, 2011; Suffczynski et al., 2014) and motor networks (Yazdan-Shahmorad et al., 2013), supporting its use as an indicator of regional excitability. Correlations were computed at each time point between -0.25 and 0 s, and for each cortical source within the right anticipatory motor network (see Table 1). A one-tailed, one-sample permutation cluster test with temporal adjacency (-0.25 to 0 s) was used to test whether stronger EMG inhibition is linked to reduced neural activity across the right anticipatory motor network.

To investigate the potential involvement of additional brain regions in the regulation of anticipatory muscle inhibition via alpha- and beta-band synchrony, we computed Spearman's rank correlations between periodic power and EMG inhibition at

each source vertex within the right anticipatory motor network, across time-frequency points in the 8-30 Hz range and the -0.25 to 0 s time window. To further assess the contribution of subcortical structures, the same correlation analysis was performed for the right cerebellum and basal ganglia. Separate one-tailed, one-sample permutation cluster tests with temporal (-0.25 to 0 s) and frequency (8-30 Hz) adjacency were conducted to determine whether stronger EMG inhibition was associated with increased alpha- and beta-band power across both the right anticipatory motor network and the subcortical regions.

To assess the relationship between alpha-beta (8-30 Hz) and high-gamma (90-130 Hz) power within the selected cluster region – while controlling for their shared variance due to broadband power fluctuations – we computed partial Spearman's correlation coefficients at each vertex using the partial_corr() function from Pingouin (v. 0.5.3), with mean total power in the 1-130 Hz range included as a covariate (Spaak et al., 2012). The resulting correlation values were then averaged across all vertices within the cluster. Although this approach has certain limitations, it allowed us to account for trial-to-trial power variability common to both frequency bands when estimating their relationship.

Mediation analysis

To further investigate the interplay between high-gamma power, periodic beta power, and EMG inhibition in the brain region where significant correlations among these measures were observed (see MEG data Results), we performed a mediation analysis. Specifically, we tested whether high-gamma power (mediator, M) mediated the

relationship between beta power (independent variable, X) and EMG inhibition (dependent variable, Y). The analysis focused on the “peak vertex” within the SMA cluster region, defined as the vertex showing the strongest correlation between high-gamma power and EMG inhibition within a cluster (see MEG data Results). Total (without aperiodic component subtraction) beta and high-gamma power were averaged over their respective frequency bands – 24-25 Hz for beta and 90-130 Hz for gamma – and across the time interval in which a significant correlation between gamma power and EMG inhibition was observed (-0.06 to -0.018 s). Notably, this time window overlapped with the interval during which beta power (24-25 Hz) was also significantly correlated with EMG inhibition (see Results and Figure 3A,B). The use of a unique time interval for estimation of both the independent variable and the mediator is justified by the fast conduction velocity of neural signals (less than 1 ms), which is below the time resolution of the current data, making it impossible to differentiate their exact timings.

The mediation analysis was performed using the mediate() function (package ‘mediation’, v. 4.5.0) in R, employing bootstrapping with 10,000 permutations to obtain robust estimates of the mediation effects. To account for random effects, a generalized additive model (GAM, function bam(), package ‘mgcv’ v. 1.9.0) with linear fixed effects (gamma power, beta power), random effects per subject (random intercepts, random beta and gamma slopes) were employed. Restricted maximum likelihood (REML) was used as the estimation method for the GAM models. The models used as inputs for the mediation analysis – models A and C’ – are described in Table 2. To justify the presence of relationships between the mediator and dependent variable, and between the

independent and dependent variables, two additional models – models B and C (Table 2) – were specified.

Model	Relationship	Formula in mgcv
A	$X \rightarrow M$	Gamma ~ Beta+s(Subject,bs='re')+s(Subject,Beta,bs='re')
C′	$X + M \rightarrow Y$	Inhibition ~ Beta+Gamma+s(Subject,bs='re')
		+s(Subject,Beta,bs='re')+s(Subject,Gamma,bs='re')
B	$M \rightarrow Y$	Inhibition ~ Gamma+s(Subject,bs='re')
		+s(Subject,Gamma,bs='re')
C	$X \rightarrow Y$	Inhibition ~ Beta+s(Subject,bs='re')+s(Subject,Beta,bs='re')

Table 2. Mediation analysis models.

Inhibition: EMG inhibition; *Gamma:* gamma power averaged over 90-130 Hz; *Beta:* beta power averaged over 24-25 Hz and adjusted for correlation with broad range total power (1-130 Hz); *s(Subject,bs='re'):* subject-based random intercept; *s(Subject,Beta,bs='re'):* subject-specific random slope for beta power; *s(Subject,Gamma,bs='re'):* subject-specific random slope for gamma power.

Before fitting the models, beta power was adjusted by regressing out (LinearRegression() function, ‘sklearn’, v. 1.4.2) the total power averaged across a broad frequency range (1-130 Hz) to mimic the partial correlation approach used for the Beta power vs. Gamma power correlation (see *Statistical analysis*). The resulting Beta power and Gamma power variables were further scaled between subjects to yield standardized mediation parameters. The linearity of the relationships between the

dependent and independent variables was visually inspected. The Durbin-Watson d-test (dwtest() function, 'lmtest' package, v. 0.9.40) was used to test for autocorrelation in the residuals of the estimated GAM models. The test indicated the presence of significant positive autocorrelation for *model a* (DW = 1.89, p = 0.01). However, the DW value is close to 2, suggesting that the autocorrelation is mild and may not substantially affect the validity of the model. For the other models, no autocorrelation was observed (mean DW ± SD: 1.970 ± 0.002, mean p-value ± SD: 0.163 ± 0.011). To assess the presence of multicollinearity among the linear predictors in *models a and c'*, the Variance Inflation Factor (VIF) was calculated (mgcv.helper::vif.gam() function, 'mgcv.helper' package, v. 0.1.9). All VIF values were < 2, suggesting an absence of multicollinearity.

Beta bursts extraction

To extract beta bursts at the vertices of interest, we employed the burst detection pipeline developed by Szul et al. (2023); https://github.com/maciekszul/burst_detection). Time-frequency decomposition and aperiodic component separation were performed using Superlets and Specparam, respectively, as described above. Unlike previous steps, a frequency resolution of 0.25 Hz was employed in the Superlet analysis to improve burst detection accuracy. Beta bursts were detected in the 10-33 Hz frequency band within a -0.8 to 0.4 s window, relative to unloading. To verify the accuracy of burst extraction, trial-wise time-frequency representations with identified bursts were visually inspected.

Bursts were extracted from the “peak vertex” within the SMA cluster region (see MEG data Results), identified as showing the strongest correlation between gamma power and EMG inhibition. For this vertex, only bursts with a burst centre frequency between 22-28 Hz and a burst centre time between -0.077 and -0.018 s were considered for analysis. The time and frequency intervals were defined based on the observed correlation between beta power and EMG inhibition: the time interval reflected the temporal effect of this correlation, while the frequency range (25 ± 3 Hz) was selected to capture the peak effect at 25 Hz. The bandwidth was kept broad enough to account for possible variability in burst waveforms, which can lead to fluctuations in frequency estimates. These bursts were individually subtracted for each trial.

Beta bursts analysis

To examine whether trials containing beta bursts within the selected time and frequency range also exhibit more pronounced anticipatory inhibition, we averaged baseline-corrected EMG power time courses (see section *Estimation of the Optimal EMG Inhibition* above) across these trials. A one-tailed, one-sample permutation cluster test with temporal adjacency was conducted across participants within the -0.25 to 0.05 s window relative to unloading onset, to assess whether EMG power was significantly reduced – i.e., whether stronger anticipatory inhibition was present in these trials relative to baseline EMG activity.

For further analysis, trials containing bursts were aligned to the center time of each burst. For the control trials, an equal number of no-burst trials were selected

based on the lowest beta power within the same time and frequency range used for burst extraction. These control trials were then aligned to the burst center times from burst trials, ensuring time shuffling in the control condition as well.

To test whether the occurrence of beta bursts was linked to high-gamma power suppression, we compared high-gamma power between trials with bursts and no-burst control trials. A one-tailed, one-sample permutation cluster test with time (-0.05 to 0.05 s around burst centers) and frequency (90-130 Hz) adjacency was conducted to assess whether the difference in high-gamma power significantly deviated from zero.

To examine whether beta bursts in the SMA are driven by input from other brain regions, we computed the Phase Slope Index (PSI), a directed connectivity measure, using the phase_slope_index() function in MNE-Python. PSI was estimated between the peak SMA vertex and all vertices within the right anticipatory motor network. Spectral decomposition for PSI calculation was performed using Morlet wavelets (4 cycles), and PSI was computed in the 22-28 Hz range separately for burst and no-burst control trials. A one-tailed spatio-temporal permutation cluster test was conducted within the -0.05 to 0 s window relative to burst centers to assess increased directed connectivity to the SMA during burst versus no-burst trials. Additional tests examined inputs from the cerebellum and basal ganglia.

We hypothesized that regions functionally connected to the SMA during beta bursts would also exhibit increased beta bursting. To test this, we assessed whether regions identified through PSI analysis showed elevated beta burst probability during SMA burst trials. Beta burst probability in these regions was calculated separately for SMA burst and no-burst control trials at each vertex, time, and frequency point, defined as the proportion of trials containing bursts at each point relative to the total number

of trials. The probabilities were then averaged across vertices within each cluster. We used a one-tailed, one-sample permutation cluster test to determine if beta burst probability (22-28 Hz) increased in PSI-defined regions during SMA burst trials relative to no-burst trials, within the -0.05 to 0.05 s window.

Statistical analysis

To check the assumptions of linear regression models, several diagnostic tests were performed. The Shapiro-Wilk test (shapiro() function, scipy.stats, v. 1.7.3) was used to assess the normality of the residuals. The Durbin-Watson test (durbin_watson() function, statsmodels.stats.stattools, v. 0.13.5) was employed to check for autocorrelation in the residuals. Homoscedasticity was tested with Breusch-Pagan Lagrange Multiplier test (het_breuschpagan() function, statsmodels.stats.api, v. 0.13.5). Multicollinearity was tested using the Variance Inflation Factor (VIF) (variance_inflation_factor() function, from statsmodels.stats.outliers_influence, v. 0.13.5).

To assess the relationship between neural activity and behavioural parameters at individual time, frequency, and spatial points, we calculated Spearman's rank correlation coefficient (spearmanr() function, scipy.stats, v. 1.7.3). Spearman's correlation was chosen due to the potential presence of non-linear relationships between the pairs of variables studied.

To perform cluster analysis, group-level statistics, or to select a common set of vertices across all subjects (e.g., the SMA cluster region or the right anticipatory motor network), timecourses or correlation coefficients computed for individual brain models

were morphed to the template brain, ‘fsaverage’, using the compute_source_morph() function in MNE-Python. For ‘fsaverage’, the BEM and source spaces were created using the same parameters as those applied to the sample data.

A non-parametric permutation cluster one-sample t-test was used for all cluster-level analyses, employing either permutation_cluster_1samp_test() for time-only data or spatio_temporal_cluster_1samp_test() for analyses involving spatial or frequency dimensions as well. A total of 1,024 permutations to build a null distribution for cluster-level inference. Clusters were formed based on adjacency in time, space, frequency, or their combinations. One- or two-tailed tests were applied according to the specific hypotheses (see respective Methods sections). Threshold-Free Cluster Enhancement (TFCE) was used for one- or two-dimensional data – time or time-frequency (starting value: 0, step size: 0.2). For higher-dimensional data involving spatial adjacency, a cluster-forming threshold based on $p = 0.001$ was used to manage computational costs. We confirmed the reliability of this approach by comparing both TFCE and cluster-based thresholding in a high-gamma/EMG correlation analysis, both of which yielded similar significant results. To stabilize *t*-statistics in the presence of low variance, the ‘hat’ variance regularization method implemented in MNE-Python was used.

Results

Behavioural data

The group-averaged elbow rotation and EMG modulation over time, including between-subject variability, are presented in Figure 2A. Distributions of Peak Elbow Rotation and Elbow Rotation Decline across trials were significantly non-normal for all participants (Shapiro-Wilk test, $p < 0.05$). Additionally, both the mean and SD were low compared to each participant's maximal elbow rotation, measured as the median of peak values during the imposed condition. The average ratio of voluntary to imposed elbow deflection was: Peak Elbow Rotation, 5.46 ± 7.44%; Elbow Rotation Decline, -0.43 ± 2.04% (see Figure 2B for individual variability). Notably, the observed 5% voluntary Peak Elbow Rotation deflection closely matches earlier findings of 8% in adults (Barlaam et al., 2012), consistent with mature anticipatory control mechanisms stabilizing forearm during voluntary load-lifting.

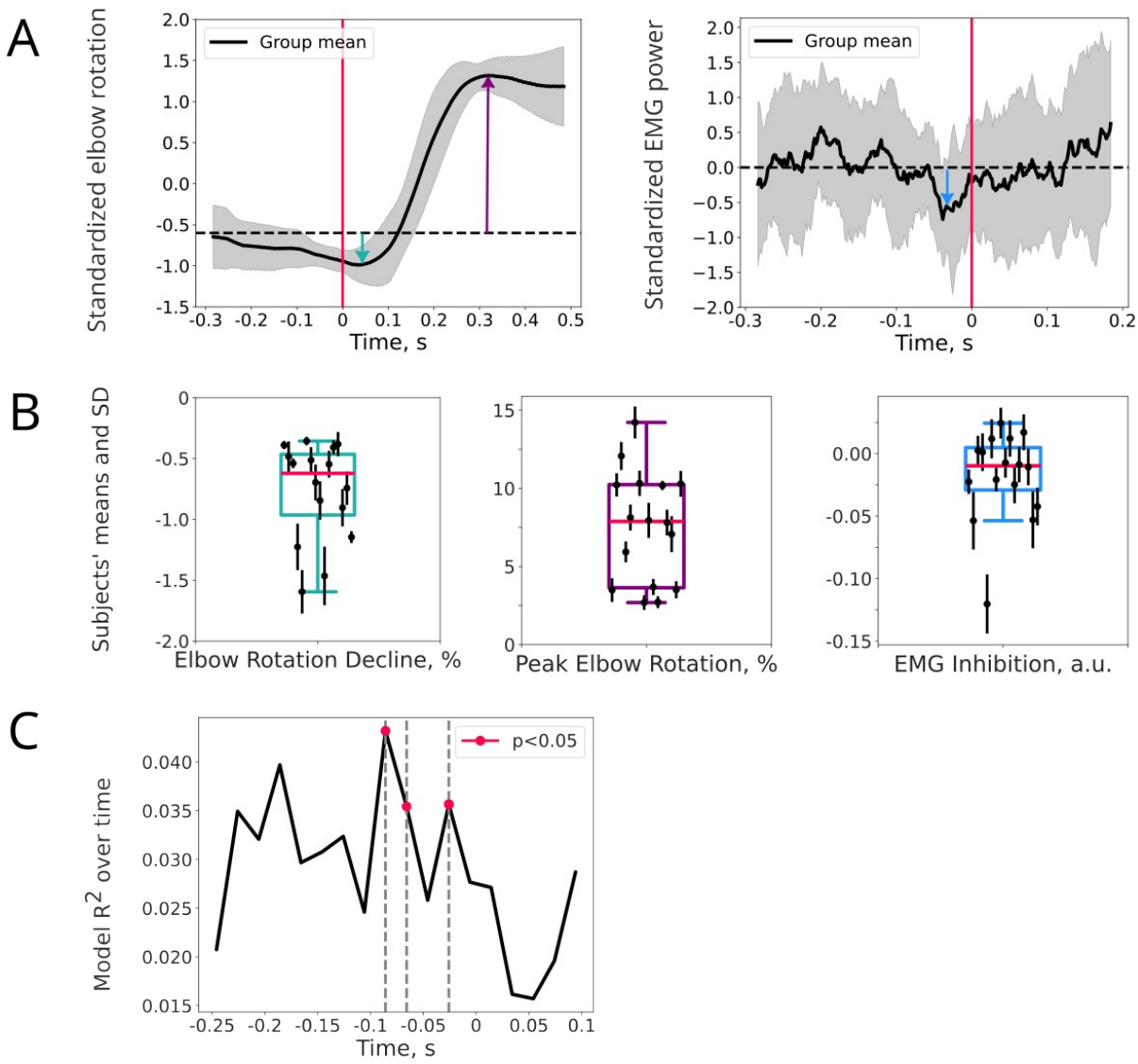

Figure 2. Behavioural analysis results. **A:** Standardized elbow rotation and *Biceps brachii* EMG aligned to unloading (vertical red line). Group means (black line) and SD (gray shading) are shown, with colored arrows indicating behavioral measures: Elbow Rotation Decline (green), Peak Elbow Rotation (purple), and EMG inhibition (blue). **B:** Participant-wise mean (dots) and SD (whiskers) values for each measure, with boxplots indicating between-subject variability. The red line marks the median, box edges show quartiles (Q1 and Q3), and whiskers extend to 1.5 times the interquartile range. **C:** Group-averaged R^2 values from linear regression models computed at each time point (dependent variable: EMG power; independent variables: Peak Elbow Rotation, Elbow

Rotation Decline). Red markers and gray dashed lines denote time points where the relationship between EMG inhibition and elbow rotation parameters reached significance.

Using within-participant variability in elbow deflection across trials, we aimed to determine the timing of anticipatory inhibition in the *Biceps brachii* that would optimize forearm stabilization. We assumed that optimal flexor inhibition timing would minimize deviations from zero in both Peak Elbow Rotation and Elbow Rotation Decline (Figure 1A; see Methods for details). Elevated Peak Elbow Rotation is likely linked to late inhibition (Barlaam et al., 2012), whereas excessive Elbow Rotation Decline might be associated with premature inhibition. Consistent with this, stronger Elbow Rotation Decline correlated with more pronounced *Biceps brachii* EMG suppression at -0.06 s and -0.08 s relative to unloading (averaged over 30 ms; $t=7.5$, $p<0.001$ and $t=5.2$, $p<0.001$, respectively). No Elbow Rotation Decline was observed in the imposed condition, where anticipatory adjustments could not occur.

To determine the optimal timing for anticipatory inhibition, we fitted linear regression models predicting *Biceps brachii* EMG over time based on trial-level variability in Peak Elbow Rotation and Elbow Rotation Decline (see Methods, section *Estimation of the EMG inhibition*). A permutation cluster test identified significant differences in baseline-corrected F-values, with the strongest effects at three time points (-0.086, -0.066, and -0.026 s relative to unloading), indicating periods when EMG modulation was most strongly associated with elbow rotation. Group-averaged R^2 values for these models are shown in Figure 2C, highlighting these three key intervals. Closer examination of the correlation coefficients between EMG power and the two

elbow rotation metrics revealed that only around -0.026 s was a stronger EMG decline associated with both reduced (less negative) Elbow Rotation Decline and lower (less positive) Peak Elbow Rotation, indicative of a more stabilized forearm. This interval also corresponded to a clear reduction in group-averaged EMG activity relative to baseline (Figure 2A, right panel), consistent with the 'on-time' inhibition scenario (Figure 1A). By contrast, earlier intervals at -0.086 s and -0.066 s showed positive associations between EMG and Elbow Rotation Decline, consistent with the 'early inhibition' scenario resulting in forearm lowering (Figure 1A).

The time interval around -0.026 s in *Biceps brachii* EMG was identified as the optimal inhibition window during the voluntary unloading task. Notably, this interval aligns with prior BLLT studies, which indicate that efficient anticipatory postural control is associated with inhibition occurring within 50 ms before unloading onset (Viallet et al., 1987). The 'on-time' inhibition measure, referred to as 'EMG inhibition' here, was calculated as the average of preprocessed (see Methods) and baseline-corrected (-1 to -0.5 s) *Biceps brachii* EMG power within a 30 ms window centered around -0.026 s. Therefore, in individual trials, stronger EMG inhibition (more negative values) not only reflects greater inhibition strength but also indicates optimal inhibition timing, whereas weaker inhibition (more positive values) suggests that inhibition occurred either too early or too late. In contrast to the elbow rotation parameters, EMG inhibition values were normally distributed (Shapiro-Wilk test, $p > 0.05$ in 14 of 16 participants) and exhibited greater variability across trials within participants (mean ± SD: -0.018 ± 0.034; see Figure 2B).

To validate the use of linear regression in this analysis, we tested if the key assumptions were met for the subject-based models at -0.026 s time point. The

linearity of the relationship between independent and dependent variables was confirmed through visual inspection of scatter plots. In all the subject-based models, the residuals were normally distributed (Shapiro-Wilk tests, $p > 0.05$ in all participants), did not show positive or negative autocorrelation supporting their independence (Durbin-Watson test, group-averaged statistics: 1.96 ± 0.19 (SD), min: 1.68, max: 2.36), and did not show the presence of heteroscedasticity (Breusch-Pagan test, $p > 0.05$ for all participants). To ensure that there was no multicollinearity, the Variance Inflation Factor (VIF) was calculated. Both independent variables had acceptable VIF values below 5, indicating that the predictors were not highly correlated (group-averaged VIF: 1.05 ± 0.05 (SD), min: 1.00, max: 1.19).

MEG data

Correlation of EMG Inhibition with contralateral anticipatory motor network dynamics

To test whether anticipatory inhibition in the *Biceps brachii* is associated with decreased excitability in a cortical region controlling the muscle, we conducted a one-sample permutation cluster test against zero on the correlations between high-gamma power (averaged over 90-130 Hz) – used as a proxy for regional excitability (Murthy and Fetz, 1996; Ray et al., 2008; Lundqvist et al., 2016; Riehle et al., 2018; Brazhnik et al., 2021) – and EMG inhibition, across vertices of the right anticipatory motor network (see Table 1). The analysis, conducted within the -0.25 to 0 s interval, revealed a significant

correlation effect, peaking in the medial frontal cortex, specifically in the SMA (Figure 3A), with the cluster spanning from -0.06 to -0.018 s (p = 0.039, corrected). This finding suggests that stronger EMG inhibition around -0.026 s relative to unloading is associated with a preceding reduction in high-gamma activity in the medial SMA, with a latency roughly consistent with previously reported neural conduction latencies (Spieser et al., 2013; Entakli et al., 2014).

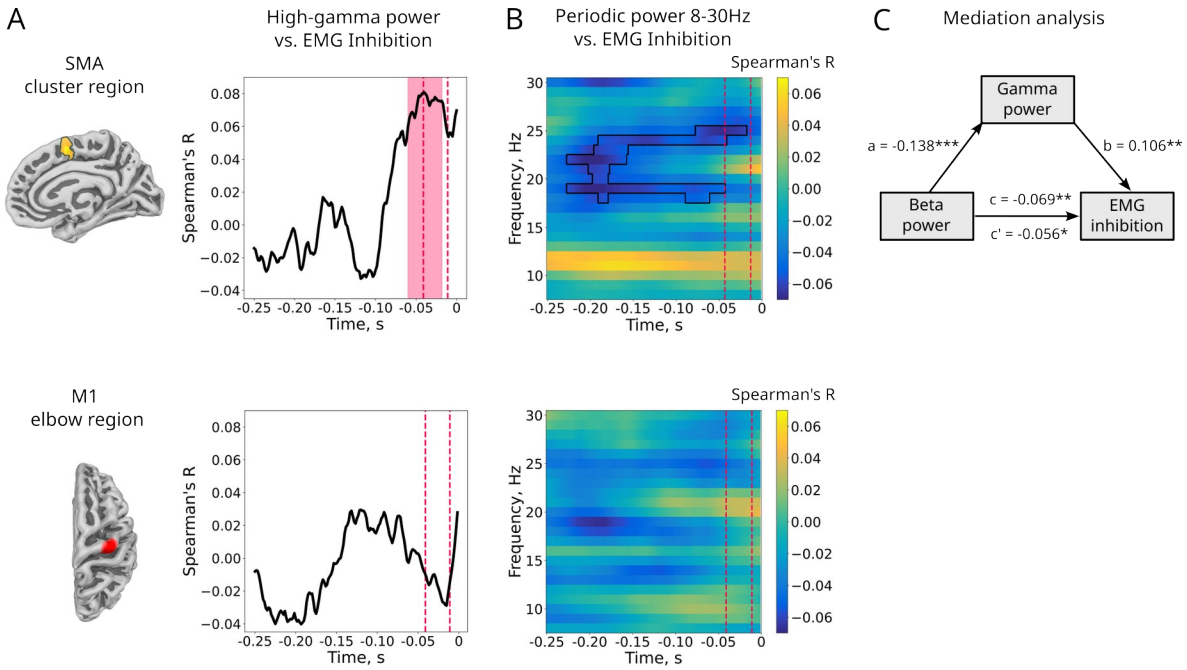

Figure 3. Neural correlates of EMG inhibition and mediation analysis. **A:** *Upper panel:* A cluster-level significant correlation effect between high-gamma power (90-130 Hz) and EMG inhibition (30 ms window centered on -0.026 s, indicated by red dashed lines) with the strongest effect observed in the medial SMA region (MNI305 peak: [8, 3, 52]). The thick black line represents the correlation time course within this cluster, with the red-shaded area highlighting its time span ($p < 0.05$, corrected). *Lower panel*: The right M1 elbow area (MNI305 peak: [32, -20, 66]) and its correlation time course, which did not

reach significance. **B:** Spearman's correlation coefficients (R) between 8-30 Hz periodic power and EMG inhibition in the SMA cluster (upper) and M1 elbow region (lower). Thin black lines indicate significant correlation effect ($p < 0.05$, corrected). **C:** Mediation analysis results showing the relationships between Beta power (independent variable), Gamma power (mediator), and EMG inhibition (dependent variable). Linear regression coefficients with the respective p-values are reported.

*p<0.05; **p<0.01; ***p<0.001

Estimating high-gamma activity in motor tasks using non-invasive methods may raise concerns about muscle activity contamination. We however argue that this is unlikely in our setup. First, MEG studies (e.g., Muthukumaraswamy, 2010) have shown detectable gamma oscillations (60-100 Hz) in motor areas like M1. Second, the anticipatory period lacked visible movement, which only became apparent after unloading began. Additionally, as described in Methods, participants exhibited minimal head motion (<1 cm), indicating limited phasic effects. While tonic muscle activity could still contribute, the use of a beamformer for source localization reduces broadband gamma artifacts (Manyukhina et al., 2022). Combined with the use of correlation as a relative measure and a spatially precise effect in the SMA, located on the medial surface where tonic muscle contamination is not expected to be strong, we claim that the observed EMG inhibition/high-gamma power correlation reflects a genuine neural process.

In contrast to the voluntary unloading condition, no significant positive correlation was observed under the imposed unloading condition between high-gamma power and the strength of the unloading reflex (EMG suppression) in the

Biceps brachii.

To further assess the contribution of other brain regions to anticipatory inhibition via alpha and beta synchrony, we computed Spearman's rank correlations between periodic power (8–30 Hz) and EMG inhibition across sources in the right anticipatory motor network and subcortical structures (basal ganglia and cerebellum). The permutation cluster test revealed no significant correlation effect between EMG inhibition and high-gamma power in either cortical or subcortical regions.

SMA cluster-based analysis

Having identified the medial SMA cluster as the most prominent cortical region where stronger EMG inhibition was linked to reduced high-gamma activity, we sought to test whether alpha- and/or beta-band rhythmic activity might mediate this inhibitory effect. Specifically, we aimed to determine whether alpha-beta periodic power correlates with both the strength of EMG inhibition and the reduction in high-gamma power within the SMA cluster.

In each of the 10 vertices within the SMA cluster, we computed Spearman's rank correlations between alpha-beta band (8-30 Hz) periodic power and EMG inhibition across time (-0.25 to 0 s) to examine whether stronger alpha-beta power was associated with more prominent EMG inhibition. A one-sample, one-tailed permutation cluster test comparing correlations against zero revealed a significant negative correlation effect, peaking in the high-beta range (18-25 Hz) and spanning -0.228 to -

0.018 s (Figure 3B). Notably, this time window overlapped with the EMG inhibition calculation period (red dashed line, Figure 3B) at 24-25 Hz, suggesting that high-beta activity may support stronger anticipatory inhibition in the *Biceps brachii*. Given the short latency between SMA stimulation and muscle response (mean MEP latency: 15.7 ms in Spieser et al. (2013); 22.6 ms in Entakli et al. (2014)), it is plausible that the observed late high-beta (24-25 Hz) effect reflects a direct inhibitory influence. By contrast, earlier lower-frequency correlations may relate to preparatory beta-band synchronization supporting inhibitory communication. However, exploring this possibility lies beyond the scope of the current study.

To investigate the relationship between late high-beta and high-gamma activity within the SMA cluster, we computed partial Spearman's correlation coefficients at each cluster vertex between 24-25 Hz power and 90-130 Hz power, averaged over both frequency and the gamma correlation time window (-0.06 to -0.018 s; Figure 3A), while controlling for broadband 1-130 Hz power to correct for shared variance from broadband fluctuations (Spaak et al., 2012). To ensure comparable estimates for both low- and high-frequency activity, we applied a common LCMV spatial filter to data filtered from 1-150 Hz. This approach revealed significantly negative individual correlation coefficients (one-sample t-test: $t = -7.16$, $p < 0.001$), indicating that stronger high-beta power was reliably linked to a more pronounced suppression of high-gamma power. A similar, albeit weaker, negative correlation was observed when periodic beta power (after removing the aperiodic component) was correlated with high-gamma power ($t = -2.17$, $p = 0.046$).

Since the relationship between EMG inhibition strength and reduced excitability was observed in the SMA, but not in M1, suggesting that the SMA mediates control

over the *Biceps brachii* to ensure forearm stabilization during voluntary unloading, we further examined whether a correlation between high-gamma and periodic alpha-beta power (8-30 Hz) and EMG inhibition could be detected in the M1 elbow region. The M1 coordinates for the left elbow area (*Biceps & Triceps brachii*) were derived from Talairach space (Lotze et al., 2000; Plow et al., 2010), converted to MNI305 space, and averaged to yield [32, -20, 66] in the right hemisphere. The M1 elbow region was defined as the peak vertex and its five adjacent vertices, forming a six-vertex M1 elbow label (see Figure 3A, lower panel). The permutation cluster test did not reveal a significant correlation between EMG inhibition and either high-gamma or 8-30 Hz power in this region.

Mediation analysis

A mediation analysis was conducted to examine whether the effect of high-beta power on EMG inhibition in the SMA is mediated through high-gamma power. To this end, data were extracted from the SMA cluster source showing the strongest correlation between high-gamma power and EMG inhibition. In the defined model, beta power was the independent variable (X), EMG inhibition was the dependent variable (Y), and gamma power served as the mediator (M). The GAM models, referred to as models A, B, C, and C' (see Methods, Mediation analysis section), included both linear fixed effects and random effects. The following significant relationships were found: beta power predicted gamma power (*model A*: estimate (β) = -0.138, standard error (SE) = 0.027, 95% confidence interval (CI) = [-0.190,-0.085], $t = -5.18$, $p < 0.001$), gamma power

predicted EMG inhibition (*model B*: β = 0.106, SE = 0.035, 95% CI = [0.037,0.175], t = 3.061, p = 0.002), beta power predicted EMG inhibition (*model C*: β = -0.069, SE = 0.025, 95% CI = [-0.120,-0.019], t = -2.725, p = 0.007), and beta power and gamma power together predicted EMG inhibition (*model C'*: beta power: β = -0.056, SE = 0.025, 95% CI = [-0.108,-0.005], t = -2.188, p = 0.029; gamma power: β = 0.092, SE = 0.035, 95% CI = [0.022,0.162], t = 2.609, p = 0.009).

The results of the mediation analysis are presented in Table 3, see also Figure 3C. The analysis revealed a statistically significant mediation effect (Average Causal Mediation Effect, ACME) of gamma power on the relationship between beta power and EMG inhibition, as well as a significant total effect. However, the direct effect (Average Direct Effect, ADE) of beta power on EMG inhibition, after accounting for the mediator, was also significant. The proportion of the total effect of beta power on EMG inhibition that was explained by the mediator accounted for 18%, suggesting a partial mediation.

	Estimate (β)	95% CI	p-value
ACME	-0.013	[-0.02, 0.00]	0.006 **
ADE	-0.057	[-0.11, -0.01]	0.027 *
Total effect	-0.069	[-0.12, -0.02]	0.007 **
Proportion mediated	0.183	[0.04, 0.67]	0.013 **

Table 3. Results of the mediation analysis examining whether the relationship between high-beta power and EMG inhibition is mediated by high-gamma power. In this model,

high-beta power (24-25 Hz) serves as the independent variable (X), EMG inhibition as the dependent variable (Y), and high-gamma power (90-130 Hz) as the mediator (M). *95% CI:* 95% Confidence Interval; *ACME:* Average Causal Mediation Effect; *ADE:* Average Direct Effect.

*<0.05, **<0.01

Beta burst analysis

Beta activity in the brain typically manifests as brief oscillatory bursts rather than sustained rhythms (Little et al., 2019; Lundqvist et al., 2024). This transient dynamic can hinder the detection of connectivity between brain areas due to the short-lived alignment of bursts (Lundqvist et al., 2024). To explore pathways potentially involved in conveying inhibitory signals to the SMA, we sought to identify brain regions communicating with the SMA in the beta band specifically during SMA beta bursts.

For this, we detected beta bursts (13-30 Hz) at the SMA cluster source showing the strongest correlation between high-gamma power and EMG inhibition. Among the detected bursts, only those centered around the time and frequency range of the correlation effect between high-beta power and EMG inhibition were selected for further analysis (–0.077 to –0.018 s, and 22-28 Hz; see Methods for details, section *Beta bursts extraction*). The percentage of trials containing such bursts was low, with a mean ± SD of 11.6 ± 1.9% per participant. The absolute number of trials with bursts was 10.1

± 1.78 (mean ± SD). Notably, the number of trials with bursts remained consistent when the time-frequency signal was extracted from the 10 vertices of the medial SMA cluster region and averaged for burst detection.

Beta bursts and EMG inhibition

The results above demonstrate that greater EMG inhibition is associated with increased high-beta power in the SMA. However, given that beta activity occurs in transient bursts, we suggested that the presence of bursts could more effectively predict the timing of anticipatory inhibition than beta power alone. To test this, we averaged baseline-corrected EMG power across trials containing bursts. A permutation cluster test comparing this averaged EMG power to zero revealed a significant decrease in EMG activity during burst trials, peaking at -0.026 s ($p = 0.008$; Figure 4A), coinciding with the predefined EMG inhibition window. In contrast, selecting an equal number of trials based on the highest beta power within the same time and frequency window yielded no significant effect ($p > 0.18$). These findings, consistent with earlier work (Little et al., 2019), suggest that the occurrence of a burst, rather than its amplitude, can better reflect its functional impact.

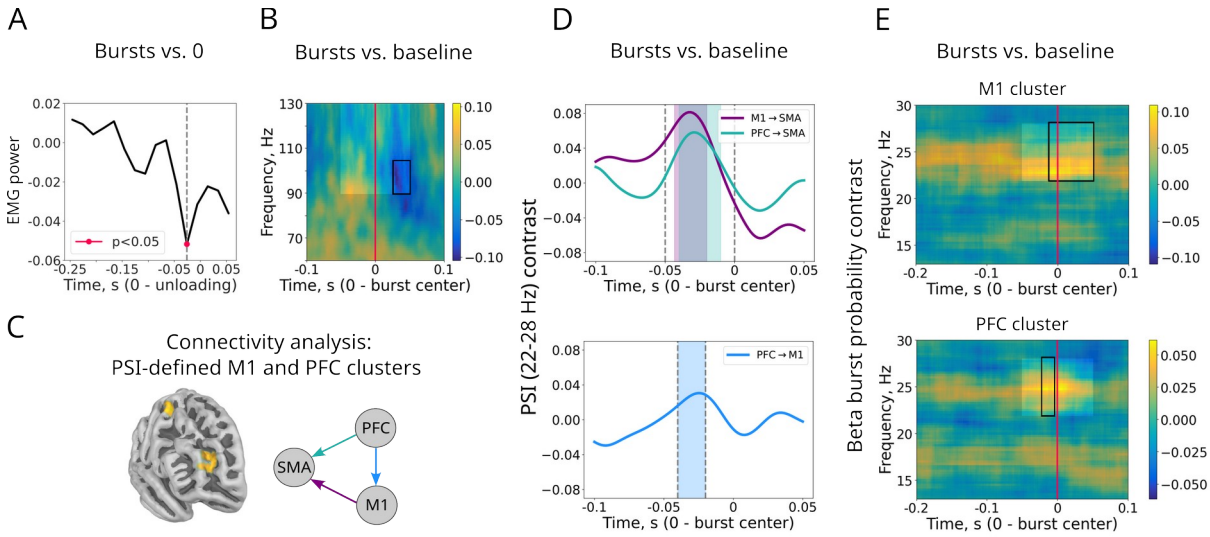

Figure 4. Beta burst analysis results. **A:** Baseline-corrected EMG power averaged across SMA burst trials. Notably, the most pronounced EMG suppression interval coincides with the previously defined EMG inhibition window. **B:** Time-frequency contrast of gamma power between SMA burst and no-burst trials. Bright rectangles indicate the analysis window, and thin black lines mark time-frequency points showing significant contrast effects ($p < 0.05$, corrected). **C:** PSI-derived connectivity cluster regions (M1: 3 vertices, MNI305 peak: [38,-8,56]; lateral PFC: 10 vertices, MNI305 peak: [31,47,11]) exhibiting increased directed connectivity toward the SMA cluster during SMA burst trials relative to no-burst trials. Connectivity directions are indicated by schematic arrows. **D:** PSI timecourses for M1-to-SMA, PFC-to-SMA, and PFC-to-M1 contrasting SMA burst and no-burst trials. In the upper panel, dashed lines outline the analysis window, with shaded areas highlighting time intervals of the most prominent effects ($p < 0.05$, corrected). The lower panel marks the overlapping period of these effects, within which the average PSI contrast was significantly different from zero. **E:** Time-frequency contrast of beta burst probability between SMA burst and no-burst trials in the M1 and PFC cluster regions. Note that for this analysis, burst probability was averaged within the 22-28 Hz frequency range. Bright rectangles indicate the

analysis window, and thin black lines mark time points showing significant contrast effects ($p < 0.05$, corrected).

Beta bursts and gamma power

We demonstrated that high-beta power negatively correlates with high-gamma activity in the SMA cluster region (Results, section *SMA cluster-based analysis*). However, since beta activity occurs in bursts, we further tested whether the presence of bursts is associated with high-gamma power suppression. A permutation cluster test confirmed a significant reduction in high-gamma power (90-130 Hz) in trials with beta bursts compared to baseline trials, in data aligned to burst centers (Figure 4B).

Connectivity analysis

To identify brain regions potentially involved in transmitting inhibitory beta bursts to the SMA, we conducted a directed connectivity analysis using the Phase Slope Index (PSI) within the burst frequency range (22-28 Hz). PSI was computed between the cortical vertices of the right anticipatory motor network (Table 1) and the SMA cluster source showing the strongest correlation between high-gamma power and EMG inhibition, separately for burst trials (data aligned to burst centers) and for baseline trials without bursts (see Methods, section *Beta Burst Analysis*).

A one-sample, one-tailed permutation cluster test revealed a significant difference in PSI between burst and no-burst trials, with two key clusters emerging: one near the M1 elbow representation ($p = 0.043$) and one in the lateral PFC (lPFC) ($p =$

0.004; Figure 4C). The PSI contrast direction indicated connectivity from these regions to the SMA. The M1 cluster was detected from -0.043 to -0.020 s, and the PFC cluster from –0.040 to -0.010 s, relative to the SMA burst center (Figure 4D, upper panel). No significant PSI differences were detected in the right basal ganglia or cerebellum.

To investigate the interaction between the PFC and M1 clusters during their concurrent influence on the SMA, we computed PSI values between these regions across vertices and time for both SMA burst and no-burst trials, and contrasted them (Figure 4D, lower panel). The PSI contrast was then averaged across the vertices and the time interval corresponding to their overlapping effect on the SMA and compared to zero across participants. This analysis revealed significant directed connectivity from the PFC to the M1 cluster (one-sample t-test, $T = 2.33$, $p = 0.034$).

To assess whether regions functionally connected to the SMA exhibit increased beta bursting during SMA bursts, we examined burst probability in the PFC and M1 clusters, averaged within the 22-28 Hz range in which connectivity was estimated. A permutation cluster test confirmed that both M1 and PFC clusters displayed higher burst probability in SMA burst trials compared to no-burst trials, with the effect most pronounced around the SMA burst centers (M1: -0.012 to 0.050 s; PFC: -0.021 to -0.005 s relative to the SMA burst center) (Figure 4E).

Discussion

In this study, we investigated the neural mechanisms underlying anticipatory muscle inhibition preventing forearm instability during voluntary load-lifting. Stronger *Biceps brachii* inhibition was linked to reduced excitability, indexed by high-gamma power, in the SMA and to increased high-beta power, with gamma suppression partially mediating this relationship. Notably, the presence of SMA beta bursts was a stronger predictor of timed inhibition than beta power alone. Together, our findings suggest that in preparation for load-lifting, high-frequency beta bursts originating from a lPFC-M1-SMA network inhibit the SMA, ultimately suppressing elbow flexor activity and stabilizing posture.

During voluntary unloading, lifting a load induces a change in force, which is counteracted by timed anticipatory inhibition restoring equilibrium. In adults, this inhibition is closely time-locked to the same muscle activation in the load-lifting arm, suggesting a central timing mechanism coordinating both arms (Paulignan et al., 1989; Massion, 1992). However, developmental studies reveal that this precise temporal coordination is acquired gradually during childhood (Schmitz et al., 2002; Barlaam et al., 2012). Bolzoni et al. (2015) further demonstrated that APA can be selectively influenced through modulation of SMA activity without affecting voluntary movement. These findings suggests that APA are governed by an independent control mechanism

that integrates both movement parameters and anticipated postural disturbances, ensuring timely adjustments to muscle tone.

Although anticipatory inhibition is well-developed in adults, its latency still exhibits some variability (Barlaam et al., 2012). We observed that optimal forearm stabilization is achieved when *Biceps brachii* inhibition precedes the onset of unloading by 26 ± 15 ms, consistent with previously reported adult latencies (25 ms: Dufossé et al. (1985); 32 ms: Barlaam et al. (2012)).

A potential association between elbow flexor inhibition and M1 excitability during BLLT was previously explored by Kazennikov et al. (2005, 2006). Using transcranial magnetic stimulation (TMS), they showed reduced M1 excitability, measured by motor evoked potentials (MEPs), during anticipatory *Biceps brachii* inhibition. However, they observed a similar positive relationship between MEP and EMG in control conditions, suggesting that this effect was not specific to APA. We estimated high-gamma (90-130 Hz) power, which closely correlates with neural spiking (Murthy and Fetz, 1996; Ray et al., 2008; Lundqvist et al., 2016; Riehle et al., 2018; Brazhnik et al., 2021), as a proxy for excitability. Surprisingly, we found no association between EMG inhibition and M1 excitability. However, stronger EMG inhibition was correlated with reduced excitability in the medial SMA – a relationship specific to the voluntary condition, as it did not appear in the imposed condition.

The involvement of the SMA in BLLT has been consistently demonstrated in MEG and fMRI studies (Schmitz et al., 2005; Ng et al., 2011, 2013a). In particular, APA impairments following contralateral SMA lesions (Viallet et al., 1992) led authors to propose that the SMA contributes to gating postural stabilization circuits – a proposition supported by the present findings. We further extend this idea, as the

observed relationship between EMG inhibition and SMA excitability suggests that the SMA directly controls *Biceps brachii* activity during load support. This control appears to be attenuated during muscle inhibition, in anticipation of force changes. Our results therefore support previous speculation by Ng et al. (2013a), who proposed that the SMA, rather than M1, might mediate APAs via direct corticospinal projections. This interpretation is supported by anatomical evidence showing that the SMA displays precise somatotopic organization (He et al., 1995; Strother et al., 2012) and has corticospinal projections about half as extensive as M1's (Dum and Strick, 1991). Additionally, TMS stimulation of the SMA during motor tasks in humans evokes arm muscle MEPs similar in latency and amplitude to those from M1 (Spieser et al., 2013; Entakli et al., 2014). These findings indicate that SMA can directly contribute to precise forearm muscles control.

In humans, SMA-originating corticospinal projections are more prominent than in non-human primates (Maier et al., 2002), which may have evolved to facilitate anticipatory control during complex hand movements (Chen et al., 2013). Such SMA-mediated hand muscle control, supported by beta-band coherence, has been demonstrated in a task requiring precise, time-predictable force production in humans (Chen et al., 2013; Spieser et al., 2013; Entakli et al., 2014). Similarly, forearm stabilization during voluntary unloading may involve partial, selective control of the elbow flexors by the SMA, the release of which facilitates a smooth transition to a new postural state. We propose that this release can be induced by inhibiting the SMA, mediated by beta bursts.

Cortical beta bursts can elicit bursts with similar characteristics in contracting muscles (Bräcklein et al., 2022) or establish between-muscle synchrony during static

postures (Simpson et al., 2024), supporting their facilitatory role in muscle control. Alternatively, indirect evidence exists suggesting that beta bursts exert an inhibitory influence on muscles, being predictive of delayed responses and action cancellation (Little et al., 2019; Wessel, 2020). Our results align with these data and demonstrate for the first time that beta-band activity, specifically bursts, can suppress muscle function. The latency of the beta correlation with muscle inhibition relative to inhibition interval (~20 ms; Fig. 3B) closely matches previously reported MEP latencies following SMA stimulation (15.7 ms, Spieser et al. (2013); 22.6 ms, Entakli et al. (2014)). Notably, this effect was partially mediated by reduced high-gamma activity, indicating that beta-related inhibition is achieved through suppression of SMA excitability. Although not always consistent (Confais et al., 2020), this aligns with previous findings of an inverse relationship between high-gamma/spiking activity and beta-band activity in sensorimotor regions (Ray et al., 2008; Lundqvist et al., 2016; Riehle et al., 2018), supporting their proposed opposing functional roles – excitatory for high-gamma and inhibitory for beta activity (Ray and Maunsell, 2011; Lundqvist et al., 2024).

If SMA beta bursts underlie anticipatory muscle inhibition, what is the source of this signal? Directed connectivity analysis in data aligned to bursts revealed that the M1 elbow area and lPFC (BA46) transmit high-beta signals to the SMA, a finding further supported by increased burst probability in both regions during SMA bursts. However, these regions seem unlikely to transmit inhibitory bursts, as neither belongs to the action cancellation network (Borgomaneri et al., 2020). The discrepancy between M1 and SMA burst effect frequencies (Figures 3B, 4E) further argues against a role for M1 in transmitting inhibitory bursts. Instead, M1 may provide proprioceptive feedback to the SMA (Nasrallah et al., 2019) or relay a copy of the motor command from the left

hemisphere (Viallet et al., 1992). In contrast, BA46 exhibits a burst effect frequency matching that of the SMA and has previously been implicated in action inhibition (Cieslik et al., 2013). Still, previous research rather suggests that this area supports the integrity and facilitates the tone of the inhibitory network in a task- and muscle-specific manner (Buschman et al., 2012; Hasan et al., 2013; Khan et al., 2024).

If neither M1 nor the lPFC transmit inhibitory bursts, which region might? Although our data cannot directly address this question, we speculate that the SMA itself could be involved. Classically, the SMA is subdivided into SMA-proper and pre-SMA (Tanji, 1994). SMA-proper is somatotopically organized, projects to the spinal cord, and connects with M1 (Coull et al., 2016) – features consistent with its proposed role in muscle control. However, SMA-proper lacks direct connections with PFC, whereas pre-SMA maintains robust connections with it, particularly BA46. Notably, pre-SMA does not project directly to M1 (Luppino et al., 1993). Functionally, the pre-SMA, alongside the IFC, constitutes a core node of the action-stopping network, supported by beta-band synchrony (Swann et al., 2012; Coull et al., 2016; Leunissen et al., 2022) and selectively suppressing motor activation patterns according to task demands (Burle et al., 2004; Carbonnell et al., 2013). Given that both SMA subdivisions contribute to motor timing (Hoffstaedter et al., 2013; Coull et al., 2016), it is plausible that pre-SMA transmits a timed inhibitory signal to SMA-proper, either directly via their adjacent arm fields (Luppino et al., 1993) or through the basal ganglia (Wadsley et al., 2022).

One limitation of this study is the inability to track individual inhibitory events in the *Biceps brachii*, which, together with a sample size limited to sixteen participants, constrains our capacity to assess the involvement of subcortical regions – specifically the basal ganglia and cerebellum – in anticipatory inhibition, given the lower signal-to-

noise ratio for deep MEG sources (Attal and Schwartz, 2013). Furthermore, although burst-centering addressed certain connectivity challenges, the variability in burst waveforms and temporal dynamics underscores the need for novel burst connectivity approaches, particularly for capturing cross-frequency interactions (Lundqvist et al., 2024).

In conclusion, our findings reveal a cortical mechanism for APA in the BLLT. We demonstrate that anticipatory *Biceps brachii* inhibition is driven by high-frequency beta bursts conveyed to the SMA, reducing its excitability and, in turn, suppressing muscle activity under SMA control. While these bursts are supported by a network involving M1 and the lPFC, further studies are needed to determine whether subcortical regions or the pre-SMA generate inhibitory bursts. Addressing this question will require time-locked analyses of individual inhibitory events and connectivity-based approaches to dissociate SMA subregions (Kim et al., 2010), while also accounting for cross-frequency burst interactions.

References

Attal Y, Schwartz D (2013) Assessment of Subcortical Source Localization Using Deep Brain Activity Imaging Model with Minimum Norm Operators: A MEG Study Barnes GR, ed. PLoS ONE 8:e59856.

Barlaam F, Descoins M, Bertrand O, Hasbroucq T, Vidal F, Assaiante C, Schmitz C (2011) Time-Frequency and ERP Analyses of EEG to Characterize Anticipatory Postural Adjustments in a Bimanual Load-Lifting Task. Front Hum Neurosci 5:163.

Barlaam F, Fortin C, Vaugoyeau M, Schmitz C, Assaiante C (2012) Development of action representation during adolescence as assessed from anticipatory control in a bimanual load-lifting task. Neuroscience 221:56–68.

Barlaam F, Fortin C, Vaugoyeau M, Schmitz C, Assaiante C (2018) Mu-oscillation changes related to the development of anticipatory postural control in children and adolescents. Journal of Neurophysiology 120:129–138.

Bolzoni F, Bruttini C, Esposti R, Castellani C, Cavallari P (2015) Transcranial direct current stimulation of SMA modulates anticipatory postural adjustments without affecting the primary movement. Behavioural Brain Research 291:407–413.

Bönstrup M, Hagemann J, Gerloff C, Sauseng P, Hummel FC (2015) Alpha oscillatory correlates of motor inhibition in the aged brain. Frontiers in Aging Neuroscience Volume 7.

Borgomaneri S, Serio G, Battaglia S (2020) Please, don’t do it! Fifteen years of progress of non-invasive brain stimulation in action inhibition. Cortex 132:404–422.

Bräcklein M, Barsakcioglu DY, Del Vecchio A, Ibáñez J, Farina D (2022) Reading and Modulating Cortical β Bursts from Motor Unit Spiking Activity. J Neurosci 42:3611.

Brazhnik E, Novikov N, McCoy AJ, Ilieva NM, Ghraib MW, Walters JR (2021) Early decreases in cortical mid-gamma peaks coincide with the onset of motor deficits and precede exaggerated beta build-up in rat models for Parkinson's disease. Neurobiology of Disease 155:105393.

Burle B, Vidal F, Tandonnet C, Hasbroucq T (2004) Physiological evidence for response inhibition in choice reaction time tasks. Brain and Cognition 56:153–164.

Buschman TJ, Denovellis EL, Diogo C, Bullock D, Miller EK (2012) Synchronous Oscillatory Neural Ensembles for Rules in the Prefrontal Cortex. Neuron 76:838–846.

Carbonnell L, Ramdani C, Meckler C, Burle B, Hasbroucq T, Vidal F (2013) The N-40: An electrophysiological marker of response selection. Biological Psychology 93:231–236.

Chen S, Entakli J, Bonnard M, Berton E, De Graaf JB (2013) Functional Corticospinal Projections from Human Supplementary Motor Area Revealed by Corticomuscular Coherence during Precise Grip Force Control Gribble PL, ed. PLoS ONE 8:e60291.

Cieslik EC, Zilles K, Caspers S, Roski C, Kellermann TS, Jakobs O, Langner R, Laird AR, Fox PT, Eickhoff SB (2013) Is There "One" DLPFC in Cognitive Action Control? Evidence for Heterogeneity From Co-Activation-Based Parcellation. Cerebral Cortex 23:2677–2689.

Confais J, Malfait N, Brochier T, Riehle A, Kilavik BE (2020) Is there an Intrinsic Relationship between LFP Beta Oscillation Amplitude and Firing Rate of Individual Neurons in Macaque Motor Cortex? Cerebral Cortex Communications 1:tgaa017.

Coull JT, Vidal F, Burle B (2016) When to act, or not to act: that's the SMA's question. Current Opinion in Behavioral Sciences 8:14–21.

Di Rienzo F, Barlaam F, Daligault S, Delpuech C, Roy AC, Bertrand O, Jerbi K, Schmitz C

(2019) Tracking the acquisition of anticipatory postural adjustments during a bimanual load-lifting task: A MEG study. Human Brain Mapping 40:2955–2966.

Donoghue T, Haller M, Peterson EJ, Varma P, Sebastian P, Gao R, Noto T, Lara AH, Wallis JD, Knight RT, Shestyuk A, Voytek B (2020) Parameterizing neural power spectra into periodic and aperiodic components. Nat Neurosci 23:1655–1665.

Dufossé M, Hugon M, Massion J (1985) Postural forearm changes induced by predictable in time or voluntary triggered unloading in man. Experimental Brain Research 60:330–334.

Dum R, Strick P (1991) The origin of corticospinal projections from the premotor areas in the frontal lobe. J Neurosci 11:667–689.

Entakli J, Bonnard M, Chen S, Berton E, De Graaf JB (2014) TMS reveals a direct influence of spinal projections from human SMAp on precise force production. Eur J of Neuroscience 39:132–140.

Enz N, Ruddy KL, Rueda-Delgado LM, Whelan R (2021) Volume of β-Bursts, But Not Their Rate, Predicts Successful Response Inhibition. J Neurosci 41:5069–5079.

Fischl B, Salat DH, Busa E, Albert M, Dieterich M, Haselgrove C, Van Der Kouwe A, Killiany R, Kennedy D, Klaveness S, Montillo A, Makris N, Rosen B, Dale AM (2002) Whole Brain Segmentation. Neuron 33:341–355.

Glasser MF, Coalson TS, Robinson EC, Hacker CD, Harwell J, Yacoub E, Ugurbil K, Andersson J, Beckmann CF, Jenkinson M, Smith SM, Van Essen DC (2016) A multi-modal parcellation of human cerebral cortex. Nature 536:171–178.

Gramfort A, Luessi M, Larson E, Engemann DA, Strohmeier D, Brodbeck C, Goj R, Jas M, Brooks T, Parkkonen L, Hämäläinen M (2013) MEG and EEG data analysis with MNE-Python. Front Neurosci 7:267.

Hasan A, Galea JM, Casula EP, Falkai P, Bestmann S, Rothwell JC (2013) Muscle and Timing-specific Functional Connectivity between the Dorsolateral Prefrontal Cortex and the Primary Motor Cortex. Journal of Cognitive Neuroscience 25:558–570.

He S, Dum R, Strick P (1995) Topographic organization of corticospinal projections from the frontal lobe: motor areas on the medial surface of the hemisphere. J Neurosci 15:3284–3306.

Hoffstaedter F, Grefkes C, Zilles K, Eickhoff SB (2013) The “What” and “When” of Self-Initiated Movements. Cerebral Cortex 23:520–530.

Hugon M, Massion J, Wiesendanger M (1982) Anticipatory postural changes induced by active unloading and comparison with passive unloading in man. Pflugers Arch 393:292–296.

Jover M, Schmitz C, Bosdure E, Chabrol B, Assaiante C (2006) Anticipatory postural adjustments in a bimanual load-lifting task in children with Duchenne muscular dystrophy. Neuroscience Letters 403:271–275.

Jover M, Schmitz C, Centelles L, Chabrol B, Assaiante C (2010) Anticipatory postural adjustments in a bimanual load-lifting task in children with developmental coordination disorder. Develop Med Child Neuro 52:850–855.

Kaluzny P, Wiesendanger M (1992) Feedforward postural stabilization in a distal bimanual unloading task. Experimental Brain Research 92:173–182.

Kazennikov O, Solopova I, Talis V, Grishin A, Ioffe M (2005) TMS-responses during anticipatory postural adjustment in bimanual unloading in humans. Neuroscience Letters 383:246–250.

Kazennikov OV, Solopova IA, Talis VL, Grishin AA, Ioffe ME (2006) Involvement of the Motor Cortex in the Bimanual Unloading Reaction: A Transcranial Magnetic

Stimulation Study. Neurosci Behav Physiol 36:177–183.

Khan AU, Irwin Z, Mahavadi A, Roller A, Goodman AM, Guthrie BL, Visscher K, Knight RT, Walker HC, Bentley JN (2024) Low-Frequency Oscillations in Mid-rostral Dorsolateral Prefrontal Cortex Support Response Inhibition. J Neurosci 44:e0122242024.

Khanna P, Carmena JM (2017) Beta band oscillations in motor cortex reflect neural population signals that delay movement onset. eLife 6:e24573.

Kim J-H, Lee J-M, Jo HJ, Kim SH, Lee JH, Kim ST, Seo SW, Cox RW, Na DL, Kim SI, Saad ZS (2010) Defining functional SMA and pre-SMA subregions in human MFC using resting state fMRI: Functional connectivity-based parcellation method. NeuroImage 49:2375–2386.

Köster M, Meyer M (2023) Down and up! Does the mu rhythm index a gating mechanism in the developing motor system? Developmental Cognitive Neuroscience 60:101239.

Leunissen I, Van Steenkiste M, Heise K-F, Monteiro TS, Dunovan K, Mantini D, Coxon JP, Swinnen SP (2022) Effects of beta-band and gamma-band rhythmic stimulation on motor inhibition. iScience 25:104338.

Little S, Bonaiuto J, Barnes G, Bestmann S (2019) Human motor cortical beta bursts relate to movement planning and response errors Ganguly K, ed. PLoS Biol 17:e3000479.

Lotze M, Erb M, Flor H, Huelsmann E, Godde B, Grodd W (2000) fMRI Evaluation of Somatotopic Representation in Human Primary Motor Cortex. NeuroImage 11:473–481.

Lundqvist M, Miller EK, Nordmark J, Liljefors J, Herman P (2024) Beta: bursts of cognition. Trends in Cognitive Sciences 28:662–676.

Lundqvist M, Rose J, Herman P, Brincat SL, Buschman TJ, Miller EK (2016) Gamma and Beta Bursts Underlie Working Memory. Neuron 90:152–164.

Luppino G, Matelli M, Camarda R, Rizzolatti G (1993) Corticocortical connections of area F3 (SMA-proper) and area F6 (pre-SMA) in the macaque monkey. J of Comparative Neurology 338:114–140.

Maier MA, Armand J, Kirkwood PA, Yang H-W, Davis JN, Lemon RN (2002) Differences in the corticospinal projection from primary motor cortex and supplementary motor area to macaque upper limb motoneurons: an anatomical and electrophysiological study. Cereb Cortex 12:281–296.

Manyukhina VO, Prokofyev AO, Galuta IA, Goiaeva DE, Obukhova TS, Schneiderman JF, Altukhov DI, Stroganova TA, Orekhova EV (2022) Globally elevated excitation–inhibition ratio in children with autism spectrum disorder and below-average intelligence. Molecular Autism 13:20.

Massion J (1992) Movement, posture and equilibrium: Interaction and coordination. Progress in Neurobiology 38:35–56.

Moca VV, Bârzan H, Nagy-Dăbâcan A, Mureșan RC (2021) Time-frequency super-resolution with superlets. Nat Commun 12:337.

Murthy VN, Fetz EE (1996) Oscillatory activity in sensorimotor cortex of awake monkeys: synchronization of local field potentials and relation to behavior. Journal of Neurophysiology 76:3949–3967.

Muthukumaraswamy SD (2010) Functional Properties of Human Primary Motor Cortex Gamma Oscillations. Journal of Neurophysiology 104:2873–2885.

Nasrallah FA, Mohamed AZ, Campbell MEj, Yap HK, Yeow C-H, Lim JH (2019) Functional connectivity of brain associated with passive range of motion exercise: Proprioceptive input promoting motor activation? NeuroImage 202:116023.

Ng THB, Sowman PF, Brock J, Johnson BW (2011) Premovement brain activity in a

bimanual load-lifting task. Exp Brain Res 208:189–201.

Ng THB, Sowman PF, Brock J, Johnson BW (2013a) Neuromagnetic imaging reveals timing of volitional and anticipatory motor control in bimanual load lifting. Behavioural Brain Research 247:182–192.

Ng THB, Sowman PF, Brock J, Johnson BW (2013b) Neuromagnetic brain activity associated with anticipatory postural adjustments for bimanual load lifting. NeuroImage 66:343–352.

Paulignan Y, Dufossé M, Hugon M, Massion J (1989) Acquisition of co-ordination between posture and movement in a bimanual task. Exp Brain Res 77:337–348.

Picazio S, Veniero D, Ponzo V, Caltagirone C, Gross J, Thut G, Koch G (2014) Prefrontal Control over Motor Cortex Cycles at Beta Frequency during Movement Inhibition. Current Biology 24:2940–2945.

Plow EB, Arora P, Pline MA, Binenstock MT, Carey JR (2010) Within-limb somatotopy in primary motor cortex – revealed using fMRI. Cortex 46:310–321.

Ray S, Crone NE, Niebur E, Franaszczuk PJ, Hsiao SS (2008) Neural Correlates of High-Gamma Oscillations (60–200 Hz) in Macaque Local Field Potentials and Their Potential Implications in Electrocorticography. J Neurosci 28:11526–11536.

Ray S, Maunsell JHR (2011) Different Origins of Gamma Rhythm and High-Gamma Activity in Macaque Visual Cortex Ungerleider L, ed. PLoS Biol 9:e1000610.

Riehle A, Brochier T, Nawrot M, Grün S (2018) Behavioral Context Determines Network State and Variability Dynamics in Monkey Motor Cortex. Front Neural Circuits 12:52.

Schaum M, Pinzuti E, Sebastian A, Lieb K, Fries P, Mobascher A, Jung P, Wibral M, Tüscher O (2020) Cortical network mechanisms of response inhibition.

Schmitz C, Jenmalm P, Ehrsson HH, Forssberg H (2005) Brain Activity During Predictable and Unpredictable Weight Changes When Lifting Objects. Journal of Neurophysiology 93:1498–1509.

Schmitz C, Martin N, Assaiante C (2002) Building anticipatory postural adjustment during childhood: a kinematic and electromyographic analysis of unloading in children from 4 to 8 years of age. Experimental Brain Research 142:354–364.

Schmitz C, Martineau J, Barthélémy C, Assaiante C (2003) Motor control and children with autism: deficit of anticipatory function? Neuroscience Letters 348:17–20.

Simpson TG, Godfrey W, Torrecillos F, He S, Herz DM, Oswal A, Muthuraman M, Pogosyan A, Tan H (2024) Cortical beta oscillations help synchronise muscles during static posture holding in healthy motor control. NeuroImage 298:120774.

Spaak E, Bonnefond M, Maier A, Leopold DA, Jensen O (2012) Layer-Specific Entrainment of Gamma-Band Neural Activity by the Alpha Rhythm in Monkey Visual Cortex. Current Biology 22:2313–2318.

Spieser L, Aubert S, Bonnard M (2013) Involvement of SMAp in the intention-related long latency stretch reflex modulation: A TMS study. Neuroscience 246:329–341.

Strother L, Medendorp WP, Coros AM, Vilis T (2012) Double representation of the wrist and elbow in human motor cortex. Eur J of Neuroscience 36:3291–3298.

Suffczynski P, Crone NE, Franaszczuk PJ (2014) Afferent inputs to cortical fast-spiking interneurons organize pyramidal cell network oscillations at high-gamma frequencies (60–200 Hz). Journal of Neurophysiology 112:3001–3011.

Swann NC, Cai W, Conner CR, Pieters TA, Claffey MP, George JS, Aron AR, Tandon N (2012) Roles for the pre-supplementary motor area and the right inferior frontal gyrus in stopping action: Electrophysiological responses and functional and structural

connectivity. NeuroImage 59:2860–2870.

Szul MJ, Papadopoulos S, Alavizadeh S, Daligaut S, Schwartz D, Mattout J, Bonaiuto JJ (2023) Diverse beta burst waveform motifs characterize movement-related cortical dynamics. Progress in Neurobiology 228:102490.

Tanji J (1994) The supplementary motor area in the cerebral cortex. Neuroscience Research 19:251–268.

Viallet F, Massion J, Massarino R, Khalil R (1987) Performance of a bimanual load-lifting task by parkinsonian patients. Journal of Neurology, Neurosurgery & Psychiatry 50:1274–1283.

Viallet F, Massion J, Massarino R, Khalil R (1992) Coordination between posture and movement in a bimanual load lifting task: putative role of a medial frontal region including the supplementary motor area. Exp Brain Res 88.

Wadsley CG, Cirillo J, Nieuwenhuys A, Byblow WD (2022) Stopping Interference in Response Inhibition: Behavioral and Neural Signatures of Selective Stopping. J Neurosci 42:156–165.

Wessel JR (2020) β-Bursts Reveal the Trial-to-Trial Dynamics of Movement Initiation and Cancellation. J Neurosci 40:411.

Xu B, Sandrini M, Wang W, Smith JF, Sarlls JE, Awosika O, Butman JA, Horwitz B, Cohen LG (2016) PreSMA stimulation changes task-free functional connectivity in the fronto-basal-ganglia that correlates with response inhibition efficiency. Human Brain Mapping 37:3236–3249.

Yazdan-Shahmorad A, Kipke DR, Lehmkuhle MJ (2013) High gamma power in ECoG reflects cortical electrical stimulation effects on unit activity in layers V/VI. J Neural Eng 10:066002.

Legends

Figure 1. Estimating elbow deflection and its expected relationship to the timing of *Biceps brachii* inhibition. **A:** Schematic illustration of three primary possible scenarios for *Biceps brachii* inhibition timing and its impact on elbow rotation. See Methods (section *Estimation of the EMG inhibition*) for a detailed explanation. **B:** Single-trial examples showing the time intervals used to estimate Peak Elbow Rotation and Elbow Rotation Decline. Values are presented as percentages of elbow rotation during voluntary unloading relative to the individual maximum, estimated as the median peak elbow rotation in the imposed condition.

Figure 2. Behavioural analysis results. **A:** Standardized elbow rotation and *Biceps brachii* EMG aligned to unloading (vertical red line). Group means (black line) and SD (gray shading) are shown, with colored arrows indicating behavioral measures: Elbow Rotation Decline (green), Peak Elbow Rotation (purple), and EMG inhibition (blue). **B:** Participant-wise mean (dots) and SD (whiskers) values for each measure, with boxplots indicating between-subject variability. The red line marks the median, box edges show quartiles (Q1 and Q3), and whiskers extend to 1.5 times the interquartile range. **C:** Group-averaged R^2 values from linear regression models computed at each time point (dependent variable: EMG power; independent variables: Peak Elbow Rotation, Elbow Rotation Decline). Red markers and gray dashed lines denote time points where the relationship between EMG inhibition and elbow rotation parameters reached significance.

Figure 3. Neural correlates of EMG inhibition and mediation analysis. **A:** *Upper panel:* A cluster-level significant correlation effect between high-gamma power (90-130 Hz) and EMG inhibition (30 ms window centered on -0.026 s, indicated by red dashed lines) with the strongest effect observed in the medial SMA region (MNI305 peak: [8, 3, 52]). The thick black line represents the correlation time course within this cluster, with the red-shaded area highlighting its time span ($p < 0.05$, corrected). *Lower panel*: The right M1 elbow area (MNI305 peak: [32, -20, 66]) and its correlation time course, which did not reach significance. **B:** Spearman's correlation coefficients (R) between 8-30 Hz periodic power and EMG inhibition in the SMA cluster (upper) and M1 elbow region (lower). Thin black lines indicate significant correlation effect ($p < 0.05$, corrected). **C:** Mediation analysis results showing the relationships between Beta power (independent variable), Gamma power (mediator), and EMG inhibition (dependent variable). Linear regression coefficients with the respective p-values are reported.

*p<0.05; **p<0.01; ***p<0.001

Figure 4. Beta burst analysis results. **A:** Baseline-corrected EMG power averaged across SMA burst trials. Notably, the most pronounced EMG suppression interval coincides with the previously defined EMG inhibition window. **B:** Time-frequency contrast of gamma power between SMA burst and no-burst trials. Bright rectangles indicate the analysis window, and thin black lines mark time-frequency points showing significant contrast effects ($p < 0.05$, corrected). **C:** PSI-derived connectivity cluster regions (M1: 3 vertices, MNI305 peak: [38,-8,56]; lateral PFC: 10 vertices, MNI305 peak: [31,47,11]) exhibiting increased directed connectivity toward the SMA cluster during SMA burst trials relative to no-burst trials. Connectivity directions are indicated by

schematic arrows. **D:** PSI timecourses for M1-to-SMA, PFC-to-SMA, and PFC-to-M1 contrasting SMA burst and no-burst trials. In the upper panel, dashed lines outline the analysis window, with shaded areas highlighting time intervals of the most prominent effects ($p < 0.05$, corrected). The lower panel marks the overlapping period of these effects, within which the average PSI contrast was significantly different from zero. **E:** Time-frequency contrast of beta burst probability between SMA burst and no-burst trials in the M1 and PFC cluster regions. Note that for this analysis, burst probability was averaged within the 22-28 Hz frequency range. Bright rectangles indicate the analysis window, and thin black lines mark time points showing significant contrast effects ($p < 0.05$, corrected).

Table 1. Regions of interest (ROIs) selected for MEG source-level analysis, representing key nodes of the right anticipatory motor network.

Primary motor cortex, M1; supplementary motor area, SMA; premotor cortex, PM; cingulate motor area, CMA; precuneus, PrCu; supramarginal gyrus, SMar; dorsolateral prefrontal cortex, dlPFC; inferior frontal cortex, IFC.

* IFC involvement was not observed in the BLLT task, however it was included in the connectivity analysis due to its well-established role in inhibitory motor control (Swann et al., 2012; Xu et al., 2016).

Table 2. Mediation analysis models.

Inhibition: EMG inhibition; *Gamma:* gamma power averaged over 90-130 Hz; *Beta:* beta power averaged over 24-25 Hz and adjusted for correlation with broad range total

power (1-130 Hz); *s(Subject,bs='re'):* subject-based random intercept; *s(Subject,Beta,bs='re'):* subject-specific random slope for beta power; *s(Subject,Gamma,bs='re'):* subject-specific random slope for gamma power.

Table 3. Results of the mediation analysis examining whether the relationship between high-beta power and EMG inhibition is mediated by high-gamma power. In this model, high-beta power (24-25 Hz) serves as the independent variable (X), EMG inhibition as the dependent variable (Y), and high-gamma power (90-130 Hz) as the mediator (M). *95% CI:* 95% Confidence Interval; *ACME:* Average Causal Mediation Effect; *ADE:* Average Direct Effect.

*<0.05, **<0.01